6-2013

Collimated blue light generation in rubidium vapor

Marcus B. Kienlen

Noah T. Holte

Hunter A. Dassonville

Andrew M. C. Dawes

Kurt D. Iverson

See next page for additional authors

Collimated blue light generation in rubidium vapor

Marcus B. Kienlen, Noah T. Holte, Hunter A. Dassonville, and Andrew M. C. Dawes
Department of Physics, Pacific University, Forest Grove, Oregon 97116

Kurt D. Iversen, Ryan M. McLaughlin, and Shannon K. Mayer
Department of Physics, University of Portland, Portland, Oregon 97203

(Received 7 June 2012; accepted 27 February 2013)

We describe an experiment for generating and characterizing a beam of collimated blue light (CBL) in a rubidium vapor. Two low-power, grating-feedback diode lasers, operating at 780.2 nm ($5S_{1/2} \rightarrow 5P_{3/2}$) and 776.0 nm ($5P_{3/2} \rightarrow 5D_{5/2}$), respectively, provide step-wise excitation to the 5D excited state in rubidium. Under the right experimental conditions, cascade decay through the 6P excited state will yield a collimated blue (420-nm) beam of light with high temporal and spatial coherence. We investigate the production of a blue beam under a variety of experimental conditions and characterize the spatial coherence and spectral characteristics. This experiment provides advanced undergraduate students with a unique opportunity to investigate nonlinear optical phenomena in the laboratory and uses equipment that is commonly available in laboratories equipped to investigate diode-laser-based absorption spectroscopy in rubidium.
[http://dx.doi.org/10.1119/1.4795311]

I. INTRODUCTION

Nonlinear optics is an important field in optical physics and one that enables a wide variety of tools and technologies. In a nonlinear material, processes such as second-harmonic generation and multi-wave mixing can be used to generate coherent light at frequencies unavailable from conventional laser sources. Nonlinear materials are particularly important in providing access to light in the UV region of the spectrum where the development of coherent sources is more difficult using traditional lasing schemes due to the extremely large pump power required to sustain a population inversion.[1]

Atomic coherence and quantum interference effects can be used to enhance nonlinear interactions between light and matter. Effects such as lasing without inversion (LWI)[1,2] and electromagnetically induced transparency (EIT)[3] have been studied actively in recent years. In LWI, quantum interference effects suppress the absorption of resonant light, making lasing possible without a traditional population inversion. Lasing without inversion was first conclusively demonstrated using the D_1 and D_2 lines in rubidium to produce laser oscillations at 794 nm.[4] Scientists continue to investigate LWI as a means of developing short-wavelength coherent sources. One example is the production of 389-nm light based on the D_1 line in cesium.[5] A related quantum interference effect, EIT, can render a normally resonant transition transparent to resonant light. Electromagnetically induced transparency has applications in LWI,[6] as well as in the reduction of the speed of light (i.e., slow light),[7] optical switches,[8,9] and all-optical wavelength converters.[10]

Frequency up-conversion is another method for producing short-wavelength sources. The generation of collimated blue light (CBL) in rubidium via frequency up-conversion was first reported by Zibrov *et al.*, who utilized low-powered, near-IR diode lasers and the 5S-5P-5D ladder transition in rubidium to produce a 15 μW, 420-nm beam with a spectral width <3 MHz.[11] Meijer *et al.* improved the up-conversion efficiency, achieving 40 μW of CBL, by detuning the two excitation lasers far from the two-step resonance and demonstrated that the collimated light exhibited a high degree of spatial and temporal coherence.[12] With careful optimization of the polarizations and frequencies of the excitation lasers, Vernier *et al.* reported generating 1 mW of CBL using the same ladder transition in rubidium.[13] This conversion efficiency far exceeds that of traditional nonlinear crystals for low power input. The generation of coherent 455-nm light has been reported in cesium vapor utilizing a similar ladder-type scheme and UV light at 330 nm (sodium) and 323 nm (lithium) has been proposed.[14] More recently, Akulshin *et al.* reported an increase in intensity and enhancement in control of the direction and divergence of the CBL in rubidium by using an additional laser for optical pumping.[15]

The alkali metal vapors have provided a rich environment for experiments in atomic and optical physics. The accessibility of electronic transitions in rubidium to resonant light from inexpensive diode laser systems has made rubidium a popular choice for laser-based atomic physics experiments in the undergraduate laboratory. Recent undergraduate-level experiments in rubidium include laser spectroscopy,[16] the temperature dependence of Doppler-broadening,[17] Faraday rotation,[18] demonstration of the Kramers-Kronig relation,[19] two-photon spectroscopy,[20] coherent population trapping,[21] and EIT.[22]

Nonlinear optics is an intriguing and important topic in modern optics. Nonetheless, undergraduate physics laboratory experiments in nonlinear optical processes are somewhat rare, due in part to the relatively high laser powers and/or expensive crystals often required to observe many nonlinear effects. Matlin *et al.* described an undergraduate laboratory in nonlinear optics where they investigate both 2-wave and 4-wave mixing in inexpensive photorefractive organic polymers.[23] Nonlinear optical phenomena can also be simulated in the undergraduate physics laboratory using Chinese tea.[24] Theoretical discussions of nonlinear optics can be found in a classic paper on second harmonic generation[25] and a discussion of degenerate 4-wave mixing can be found in the work by Ghosh *et al.*[26]

In this paper, we describe an experiment for generating and characterizing CBL in rubidium vapor, bringing a contemporary topic in nonlinear optics research into the undergraduate laboratory. We provide a detailed description of the experimental procedure and equipment, including references

for commercial suppliers,[27] and include some typical experimental results. We report on the results of experiments carried out in two different laboratories with different equipment thereby addressing a wide range of possible experimental conditions. The CBL experiment presented here uses the same equipment as saturated absorption spectroscopy[16] and two-photon spectroscopy[20] in rubidium and can therefore be easily performed in laboratories with apparatus for these experiments.

II. THEORY

The optical transitions relevant to the production of CBL in rubidium are illustrated in the partial energy-level diagram shown in Fig. 1. Two lasers, tuned to the $5S_{1/2} \rightarrow 5P_{3/2}$ (780.2-nm) and $5P_{3/2} \rightarrow 5D_{5/2}$ (776.0-nm) transitions, excite atoms to the $5D_{5/2}$ excited state. The long lifetime of the $5D_{5/2}$ state ($\tau = 240$ ns) allows for a large fraction of the population to build up in the $5D_{5/2}$ state. Atoms can decay through the $5P_{3/2}$ intermediate state ($\tau = 26$ ns) emitting near-IR light or through the $6P_{3/2}$ intermediate state ($\tau = 112$ ns) emitting IR light at 5.2 μm and blue fluorescence at 420 nm. Blue fluorescence can be observed for both co- and counter-propagating pump beams under a wide range of experimental conditions (cell temperature, laser detuning, laser power, etc.). However, using co-propagating pump beams and the right experimental conditions, a collimated blue (420-nm) beam with a high degree of spatial and temporal coherence can be produced. The process responsible for the generation of CBL has been described theoretically via the nonlinear optical process of four-wave mixing.[28]

In a nonlinear material, the polarization can be expressed as a series of terms given by[29]

$$P = \varepsilon_0 \chi E + 2dE^2 + 4\chi^{(3)}E^3 + \cdots, \tag{1}$$

where ε_0 is the permittivity of free space, χ is the electric susceptibility, E is the electric field, and coefficients d and $\chi^{(3)}$ describe the second- and third-order nonlinear effects, respectively. In a linear, non-dispersive, isotropic, homogeneous dielectric material the higher-order terms in Eq. (1) are zero so the polarization is simply proportional to the electric field $P = \varepsilon_0 \chi E$. In a nonlinear material, the second term in Eq. (1) represents the second-order nonlinearity of the material and gives rise to effects such as second-harmonic generation, the electro-optic effect, and three-wave mixing. In a material with inversion symmetry, the coefficient d vanishes and the third-order term is the lowest nonlinear term.[29] In this case, the nonlinearity can be expressed simply as $P_{NL} = 4\chi^{(3)}E^3$.

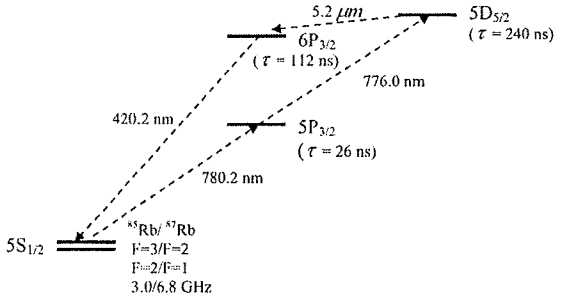

Fig. 1. Partial energy level diagram for rubidium.

Third-order nonlinearity is responsible for processes such as third-harmonic generation, the optical Kerr effect, coherent Stokes and anti-Stokes Raman spectroscopy, and four-wave mixing.

In four-wave mixing, three optical fields couple in a $\chi^{(3)}$ medium to produce a fourth coherent light field. Most generally, three distinct laser fields are combined in a nonlinear material to generate the fourth optical field. However, in this rubidium system, the two laser fields are combined in the rubidium vapor, and the third field is produced by amplified spontaneous emission arising from the population inversion in the $5D_{5/2} \rightarrow 6P_{3/2}$ transition.[28]

Energy conservation dictates that the frequencies of the four light fields are related by the frequency-matching condition $\omega_1 + \omega_2 = \omega_3 + \omega_4$, whereas momentum conservation requires the phase-matching relation $\vec{k}_1 + \vec{k}_2 = \vec{k}_3 + \vec{k}_4$. In the rubidium system, the phase-matching condition is satisfied by the relationship $\vec{k}_{780} + \vec{k}_{776} = \vec{k}_{IR} + \vec{k}_{BL}$, where $\vec{k}_{780}$ and $\vec{k}_{776}$ are the two incident laser beams at 780 nm and 776 nm, respectively, $\vec{k}_{IR}$ is the light field produced by amplified spontaneous emission from the population inversion on the $5D_{5/2} \rightarrow 6P_{3/2}$ transition, and $\vec{k}_{BL}$ is the 420 nm blue beam. The phase-matching condition is satisfied in this system when the two incident light fields co-propagate and the CBL is produced in the forward direction. It is interesting to note that since we observe on-axis wave mixing, the energy conservation equation is nearly equivalent to the phase-matching condition. That is because the index of refraction is near unity for all wavelengths involved.

Consideration of the phase-matching condition provides students with a framework for thinking about nonlinear optical processes and puts the process in the context of physical principles commonly encountered in the undergraduate physics curriculum. Detailed analysis of CBL generation in rubidium is complicated due to the presence of multiple atomic hyperfine and Zeeman sublevels, Doppler-broadening, and competing processes such as single-photon absorption, two-photon absorption, and fluorescence. Theoretical analysis of the rubidium system can be performed using the density matrix formalism.[30] While comprehensive analysis using this method is beyond the scope of most undergraduate courses, a brief overview of the process and summary of the general results can provide students with insight into how this type of problem can be analyzed in detail. The interested reader is referred to the work of Meijer,[12] Vernier,[13] and Morigi[31] for a more detailed theoretical analysis.

The density matrix formalism is a semi-classical approach to characterizing light-atom interactions where the laser fields are treated as classical plane-waves and the atom is modeled quantum mechanically. To analyze the behavior of the system, the density matrix elements are determined from the Liouville equation of motion (i.e., Schrodinger's equation expressed in terms of the density operator ρ)[30]

$$\dot{\rho} = -\frac{i}{\hbar}[H, \rho], \tag{2}$$

where the Hamiltonian H describes the coupling between the atomic states and the applied electric field. The decay of the atomic levels due to spontaneous emission can be incorporated by adding a decay term to the density operator equation, giving

$$\dot{\rho} = -\frac{i}{\hbar}[H, \rho] - \frac{1}{2}\{\Gamma, \rho\}, \tag{3}$$

where $\{\Gamma, \rho\} = \Gamma\rho + \rho\Gamma$ and Γ is a matrix that describes the relaxation processes.[30] The ijth matrix element of the density matrix equation is then given by the equation

$$\dot{\rho}_{ij} = -\frac{i}{\hbar}\sum_k (H_{ik}\rho_{kj} - \rho_{ik}H_{kj}) - \frac{1}{2}\sum_k (\Gamma_{ik}\rho_{kj} + \rho_{ik}\Gamma_{kj}). \tag{4}$$

The steady-state solution for the density matrix ρ yields information regarding the state of the system. The on-diagonal density matrix elements correspond to the probability of being in a particular state, and the off-diagonal elements describe the coherence associated with the transition and are proportional to the electric dipole moment of the transition. The off-diagonal elements of the density matrix determine the polarization P and the electric field and polarization are linked by Maxwell's wave equation, which is expressed in a nonlinear medium as

$$\nabla^2\vec{E} - \frac{1}{c^2}\frac{\partial^2\vec{E}}{\partial t^2} = \mu_0\frac{\partial^2\vec{P}}{\partial t^2}. \tag{5}$$

The steady-state solution of the density matrix equation for a four-level atomic system can be found in the work of Morigi *et al.*[31] These authors use the density matrix approach to calculate the steady-state solution for the rubidium ladder system for four (5S, 5P, 5D, 6P), five [5S (F = 2, 3), 5P, 5D, 6P], and sixteen (all hyperfine states) levels and their analysis indicates the possibility of strong gain on the 420-nm transition.[12] A summary of some of the parameters that impact CBL production is provided below.

The efficiency of the frequency up-conversion process depends significantly on the population of the 5D excited state. This state can be reached via step-wise excitation through the intermediate 5P state or via two-photon excitation provided the sum of the two laser frequencies corresponds to that of the $5S_{1/2} \rightarrow 5D_{5/2}$ transition. Two photon absorption using even a single laser is relatively efficient for this ladder transition in rubidium due to the near coincident wavelengths (2 nm detuning) of the two transitions; however, excitation to the 5D state is significantly enhanced when the two pump lasers are resonant with the intermediate 5P state.[32]

In a Doppler-broadened media, step-wise excitation from the ^{85}Rb $5S_{1/2}F = 3$ ground state excitation can occur through one of three intermediate 5P hyperfine states ($F' = 2, 3, 4$) (ignoring the hyperfine levels of the 5D state). The only true cycling transition is the $5S_{1/2}(F = 3) \rightarrow 5P_{3/2}(F' = 4)$ transition since optical pumping to the $F = 2$ hyperfine ground state tends to depopulate the other states. Thus, excitation through the $5P_{3/2}(F' = 4)$ state is the most efficient means of populating the 5D state. Furthermore, because the efficiency of the process depends on the distribution of atoms among the hyperfine and magnetic sub-levels of the states, the polarization of the pump lasers will impact CBL production. Just as the excitation efficiency to the 5D state is maximized by transitions among hyperfine levels of maximum hyperfine level F, optimal excitation to the 5D state will occur among magnetic sublevels of maximum m_F.[28] This situation can be achieved by using pump lasers with the same circular polarization.

The temperature of the cell will also play an important role in the process of CBL production. At higher cell temperatures, more rubidium atoms will be found in the vapor; however, this may not result in a straightforward increase in CBL production as there will also be an increase in absorption of the 780-nm light along the length of the cell. Analysis of the density matrix suggests that a significant enhancement in CBL production can be achieved by detuning the 780-nm laser to a frequency between the two hyperfine ground states.[12,28] This detuning should increase the transmission of the 780-nm beam along the cell and provide for longer interaction region for excitation to the 5D state.

The CBL produced in this ladder transition in rubidium has been shown to exhibit a high degree of temporal and spatial coherence.[12] The experiment can therefore provide students with a valuable opportunity to explore the topic of optical coherence. The coherence properties of an optical source can be classified in terms of the temporal and spatial coherence. The temporal coherence is a measure of the frequency bandwidth $\Delta\nu$ of the source. For a purely monochromatic source, the frequency bandwidth is zero and the corresponding coherence time ($\Delta t_c = 1/\Delta\nu$) and coherence length ($c\Delta t_c$) are infinite. For a polychromatic source, the coherence time and coherence length, respectively, provide a measure of the time interval and distance over which points on the wave have a fixed (predictable) phase relationship relative to one another. Highly monochromatic sources, such as lasers, have a narrow spectral linewidth and a correspondingly long coherence length, with typical values of coherence length on the order of a few meters. This high degree of temporal coherence makes laser sources handy tools for interference experiments. The degree of temporal coherence exhibited by a partially coherent source can be measured using a Michelson or Mach-Zehnder interferometer wherein a wave interferes with a copy of itself that is time delayed due to the difference in optical path length between the two interfering beams. Interference fringes will be visible for optical path differences less than the coherence length.

For a "point source" all waves emanate from the same physical location. For a real optical source of finite extent, waves emanate from different lateral positions. The spatial coherence of an optical source is a measure of the lateral extent over which points along the wavefront have a fixed phase relationship with one another and can thereby demonstrate interference effects. The spatial coherence of an optical source can be investigated by observing the double-slit interference pattern for different slit spacings.

III. EXPERIMENTAL APPARATUS

This experiment was carried out in two laboratories on different campuses. A diagram of the common experimental setup is shown in Fig. 2. In both experiments, the two lasers were hand-built, grating-feedback, extended-cavity diode lasers operating in a Littrow configuration.[33–35] The laser injection current was provided by a low noise current-control circuit[36] and temperature control was provided by a Peltier element and temperature-control circuit.[37] Grating-feedback diode laser systems provide reliable, tunable (3–10 GHz), narrow-band (<1 MHz) laser light at low cost and are suitable for construction by undergraduates.[16,33–35,38] Tunable diode lasers, current-control circuits, and temperature-control circuits with similar characteristics are also commercially available.[39]

Two different types of diodes were used: Hitachi model HL 78516 and Roithner LaserTechnik ADL 78901TX. The

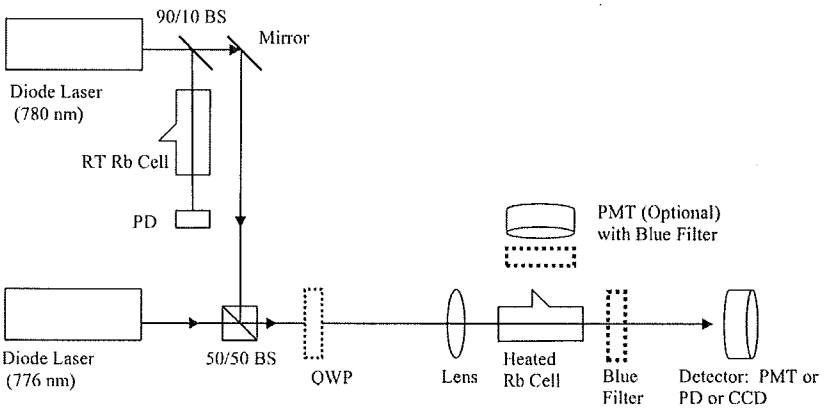

Fig. 2. Experimental apparatus. Components include grating-feedback diode lasers, quarter-wave plate (QWP), beam splitter (BS), lens, rubidium cell (heated and room temperature), 420-nm bandpass filter, photodetector (PD), and photomultiplier tube (PMT).

laser diodes have a typical free-running wavelength of approximately 785 nm and specified maximum optical power of 50 and 90 mW, respectively. The laser beams were nominally linearly polarized upon exiting the lasers. The subsequent polarizations of the two beams were independently adjusted using quarter-wave plates (Meadowlark Optics RQM-100-0780). The beams were aligned to co-propagate and were then focused into a rubidium cell using a converging lens. The rubidium vapor cell had optical quality windows and contained natural rubidium (72% ^{85}Rb, 28% ^{87}Rb). The rubidium cells used in the experiments differed slightly from one another. In the Mayer laboratory, the rubidium vapor cell was 100 mm long with parallel windows (Opthos Instruments). In the Dawes laboratory, the rubidium cell was 75 mm long and had angled quartz windows set at 11° (Triad Technology TT-RB-75-V-Q). In both cases, the cell was heated using a simple hand-built cylindrical oven and the temperature was monitored using a thermocouple probe placed in contact with the cell near the center. The Mayer oven was comprised of an aluminum tube wrapped with heat tape. Holes in the tube provided optical access for the laser beams as well as for observation of blue florescence from the side. To prevent rubidium vapor from condensing on the cell windows, they were kept hotter than the center of the rubidium cell. The Dawes oven utilized a pair of flexible polyimide film heaters (Omega, KHLV-103/5-P) mounted to a tube of magnetic shielding foil (CO-NETIC material, 0.004 in. thickness). The heater and CO-NETIC foil are wrapped around the Rb vapor cell.

The laser power was measured using an optical power meter (Thorlabs S120A with S110 detector or Thorlabs PM100D with S1120C detector). In the Mayer laboratory, the maximum power at the entrance face of the rubidium vapor cell was 8.5 mW and 9.0 mW at 780 nm and 776 nm, respectively. The cross sections of the laser beams were elliptical with dimensions 11 mm × 3.5 mm and 7 mm × 2.5 mm, respectively, for the 780-nm and 776-nm lasers. The beams were focused into the cell using the 250-mm lens. The maximum power measured at the entrance face of the vapor cell in the Dawes laboratory was 21 mW and 13.8 mW at 780 nm and 776 nm, respectively. The cross sections of the laser beams were nearly circular with a diameter of 1 mm in both beams. The beams were focused into the cell using a 90-mm lens. The different beam parameters (width and focus) between the laboratories result in slightly different beam intensity throughout the cell. In particular, the Mayer laboratory setup uses a higher focal intensity but a lower average intensity compared to the Dawes laboratory. We find that the CBL process, while intensity dependent, can be observed over a wide variety of beam parameters. For narrow beams, such as those used in the Dawes laboratory, careful alignment of the co-propagating pump beams becomes more important for maximizing the CBL power.

A 90/10 beam-splitter diverted a portion of the 780-nm beam to a second rubidium cell and onto a homebuilt silicon photodetector (photodiode: Thorlabs FDS100) that provided a frequency reference. By monitoring for blue fluorescence from the 5D-6P-5S decay at 420 nm, the frequency of the 776-nm laser was determined.

The frequency of the 776-nm laser was set to the $5P_{3/2} \rightarrow 5D_{5/2}$ transition wavelength using temperature and current adjustments. The 780-nm laser beam was scanned in frequency 3–10 GHz across the $5S_{1/2} \rightarrow 5P_{3/2}$ Doppler-broadened absorption profile by driving a piezoelectric transducer in the flexure of the laser assembly. The laser wavelength was monitored using a wavelength meter with 0.01 nm resolution (Burleigh WA-2500 Wavemeter Jr. or Bristol 512-VIS).

While the Doppler-broadened absorption profile of the 780-nm laser beam was monitored, the collimated blue beam was simultaneously measured using a photo-multiplier tube (PMT Burle 931A, Mayer laboratory) or amplified photodiode (Hamamatsu S5971, Dawes laboratory), with a 420-nm bandpass filter (Thorlabs FB420-10). Blue fluorescence from the cell was easily observable in a dark room at cell temperature above approximately 60 °C. The collimated blue beam was characterized using a variety of optical detectors (PMT, silicon photodetector, optical power meter, CCD camera, and spectrometer) under various experimental conditions including different combinations of laser power, polarization, and pump laser frequency.

As a final note on the experimental setup, it is tempting to split the output with a beamsplitter in order to observe the CBL with a CCD and PD/PMT simultaneously. While this is advantageous for simply observing the effect, we caution that most beamsplitters are designed or AR coated for a particular wavelength range. The output and pump beam wavelengths differ by hundreds of nm so the performance of wavelength dependent devices must be considered. In

particular, $\lambda/2$-thickness AR coatings designed for 780 nm are highly reflective at 420 nm where they are $\sim\lambda$ thick.

IV. EXPERIMENTAL RESULTS AND DISCUSSION

The process of CBL generation is very robust and observable over wide range of experimental conditions; however, because there are several competing and complicated processes at work, many experimental factors impact CBL production. Easily adjustable parameters include the pump laser powers, beam polarization, frequency detuning, alignment and collimation, and the temperature of the vapor cell. The impact of these parameters on CBL production provides for a wealth of experimental investigations. Some typical experimental results are described below.

A sample output spectrum from the rubidium cell is shown in Fig. 3. Taken using StellarNet Spectrometer EPP2000, the spectrum shows the blue beam at 420 nm generated within the cell along with the incident laser beams at 776 and 780 nm. Similar results were observed using an Ocean Optics Red Tide USB650 spectrometer. The near-IR beams were attenuated after the cell so that all three beams could be displayed on the same graph; the actual power of the near-IR lasers is much larger than that of the blue beam. All other data were collected with the blue bandpass filter positioned at the exit end of the cell to attenuate the near-IR laser beams by 40 dB. Accurate measurement of the CBL linewidth was limited by the resolution of the spectrometer.

The CBL was found to be highly collimated with a typical beam divergence of 3–4 mrad. The spatial coherence of the blue beam was investigated via two-slit interference as shown in Fig. 4. The interference pattern was generated by sending the blue beam through a double slit (slit separation 0.25 mm; slit width 0.04 mm). The wavelength of the blue beam was measured from the double-slit pattern to be 431 ± 10 nm. The blue interference pattern, clearly visible on a white screen in a dark room, was recorded using a black-and-white CCD camera. High contrast fringes were observable out to order 22, suggesting a high degree of spatial coherence. Similar fringes, with less contrast, are clearly visible even at low pump-laser powers. The temporal coherence of the beam could be characterized using a Michelson interferometer.

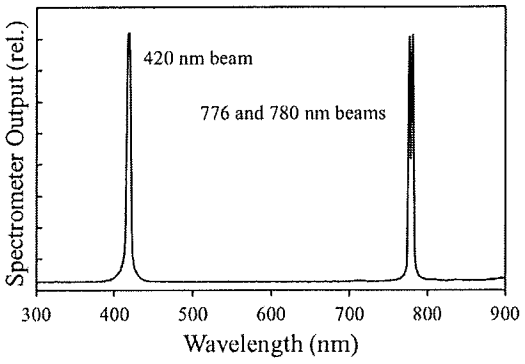

Fig. 3. Sample output spectrum from the heated rubidium cell taken using a StellarNet EPP2000 spectrometer. The spectrum shows the blue beam at 420 nm generated within the cell along with the incident (much stronger) laser beams at 776 nm and 780 nm. The near-IR beams were attenuated so that all three beams could be displayed on the same graph.

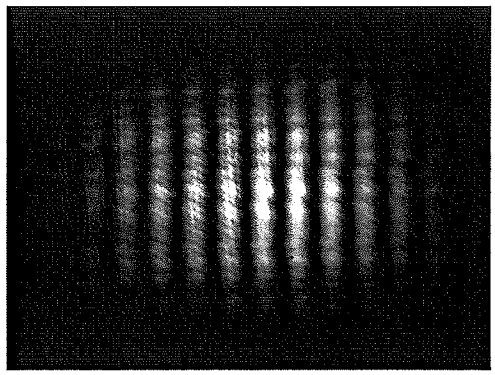

Fig. 4. Interference pattern of the blue beam through a double-slit aperture with slit separation of 0.25 mm. The interference pattern was monitored using a black and white CCD camera.

Without the bandpass filter in place a diffraction grating can be used to produce diffraction peaks on the screen simultaneously for the blue and near-IR beams. The colorful display reinforces to students the wavelength dependence of the peak spacing.

The CBL power was characterized as a function of the frequency of the pump lasers, cell temperature, and the incident laser beam power and polarization. Figure 5(a) shows a sample PMT signal as the 780-nm laser was scanned over the ^{85}Rb (F = 3) and ^{87}Rb (F = 2) ground-state transitions. The

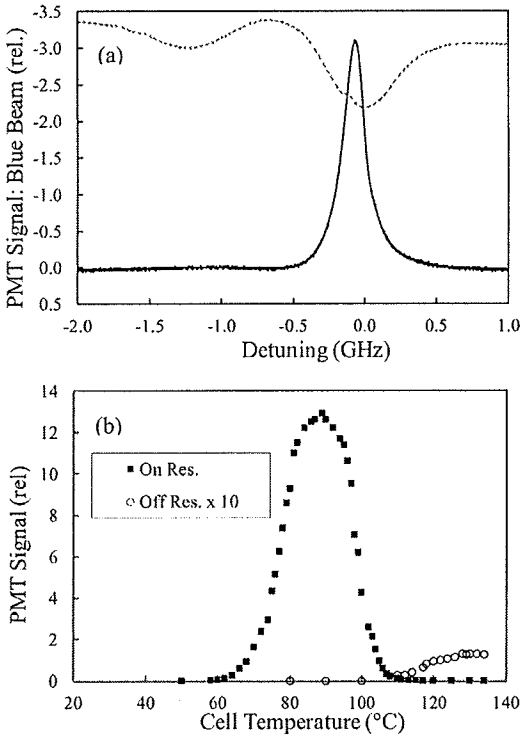

Fig. 5. (a) Sample PMT signal (solid line) of the "on-resonance" collimated blue beam as the 780-nm laser is scanned over the ^{85}Rb (F = 3) and ^{87}Rb (F = 2) ground-state transitions. The laser powers were 8.5 mW and 8.9 mW, respectively, for the 780-nm and 776-nm laser beams. The rubidium absorption spectrum of the 780-nm laser (dashed line), taken in a room temperature cell, is included for reference. (b) Collimated blue-beam power as a function of cell temperature for the "on-resonance" (squares) and "off-resonance" (circles) beam.

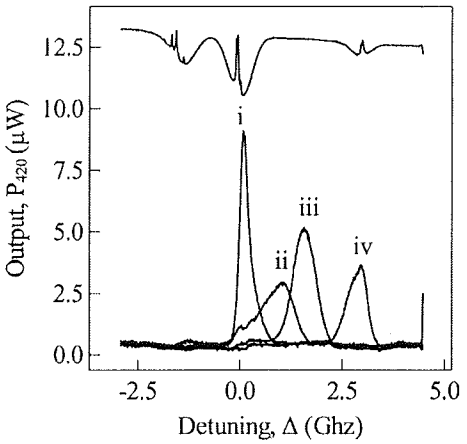

Fig. 6. Photodetector signals for the collimated blue beam as the 780-nm pump laser scans through the D_2 resonance at a cell temperature of T = 87 °C. Approximate detuning (Δ_{776}) is: (i) 0 GHz, (ii) −1 GHz, (iii) −1.6 GHz, (iv) −2.9 GHz. The rubidium absorption spectrum of the 780-nm laser (upper trace), taken in a room temperature cell, is included for reference.

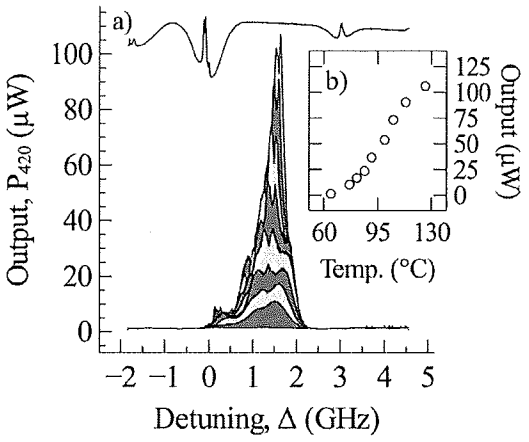

Fig. 7. (a) Sample photodetector signals of the "off-resonance" collimated blue beam at a variety of temperatures as the 780-nm laser is scanned over three of the rubidium hyperfine ground states. The laser powers were 21 mW and 13.8 mW, respectively, for the 780-nm and 776-nm laser beams. The rubidium absorption spectrum is included for reference. (b) Collimated blue-beam power as a function of cell temperature for the "off-resonance" beam.

frequency of the 776-nm laser was set to optimize the CBL power and fixed (not scanning). Figure 5(b) (solid squares) displays the peak blue-beam power as a function of cell temperature for the "on-resonance" blue beam shown in Fig. 5(a). At higher cell temperatures, absorption of the 780 nm pump beam diminished the 2-photon process leading to decreased power in the generated blue beam. Above 110 °C a smaller "off-resonance" peak appeared (unfilled circles). An output of 15 μW was achieved in the Mayer laboratory at a cell temperature of 89 °C for incident laser powers of 8.5 and 9.0 mW at 780 and 776 nm, respectively.

At cell temperatures between 70 °C and 110 °C, we observe collimated blue light for on- and off-resonance detunings of the 780 nm pump laser. Figure 6 includes four example scans of the 780-nm laser for various 776 nm pump detunings. At 87 °C, the maximum CBL effect occurs when the 780-nm pump is tuned to resonance. An off-resonance effect is also observed for a variety of pump detunings. We find the off-resonance CBL process is most efficient for a pump laser detuning $\Delta_{780} = -\Delta_{776}$ of approximately 1.6 GHz (relative to the ^{85}Rb F = 3 ground state) corresponding to Fig. 6(iii), in agreement with prior observations.[12,13]

The off-resonance peak was investigated in greater detail in the Dawes lab; this was made easier due to the larger scanning range of the 780-nm laser and higher power of the two pump lasers. Figure 7(a) shows the photodetector signal as the 780-nm laser was scanned over three of the four ground state hyperfine transitions in rubidium and the frequency of the 776-nm laser was fixed. As shown, the peak power increases with temperature from 60 °C through 130 °C. Above this temperature, the output power decreases smoothly and symmetrically about 130 °C. Figure 7(b) shows the peak blue-beam power as a function of cell temperature for the off-resonance blue beam. An optimum off-resonance signal of 110 μW was achieved at a cell temperature of 127 °C for incident lasers power of 21 mW and 13.8 mW at 780 nm and 776 nm, respectively. The off-resonance peak was observed in both laboratories with approximately the same temperature dependence, though the power was significantly higher in the Dawes laboratory. The off-resonance configuration has been shown by others to significantly enhance the generation of collimated blue light because single-photon absorption and nonlinear self-focusing of the 780-nm laser beam are minimized off resonance.[12,13]

Figure 8 shows the relative power of the blue beam as a function of the incident laser beam powers. Figure 8(a) shows the results for the on-resonance peak in the Mayer laboratory. Figure 8(b) shows the results for the off-resonance peak in the Dawes laboratory. Figure 8(c) is a log-log plot of the data from Fig. 8(b). In each case, the squares (circles) correspond to adjusting the 780 nm (776 nm) laser power with the 776 nm (780 nm) laser power fixed. The dashed line, provided for reference in Fig. 8(c), corresponds to an $x^{1.5}$ power dependence. For the on-resonance effect, and in the low-power regime, the output increases with increasing pump power regardless of which pump laser is adjusted [see Fig. 8(a)]. Below 5 mW, the output power increases nonlinearly with pump power, but above 5 mW, the relationship is approximately linear. Compared to the on-resonance case, the off-resonance effect is more dependent on the power of the 776-nm pump laser than on the power of the 780-nm laser. This observation is in agreement with prior studies on CBL generation (as an example, see Fig. 3 in Ref. 13).

The polarization of the two near-IR pump lasers had a significant impact on the output power of the CBL. Figure 9(a) shows sample PMT signals for the on-resonance blue beam as the 780-nm laser was scanned in frequency over the ^{85}Rb (F = 3) and ^{87}Rb (F = 2) ground state transitions. Figure 9(b) shows the corresponding PMT signal of the blue fluorescence measured from the side of the cell. The results show that the blue-beam power is strongly dependent on the pump laser polarization. The optimum blue-beam power was observed when the two incident beams had the same circular polarization. Parallel (crossed) linear polarizations yielded a blue beam of approximately forty (twenty) percent power. Opposite circular polarizations essentially eliminated the collimated blue beam, though the blue fluorescence signal was still clearly visible in the cell with this configuration of polarizations. Figure 9(c) shows a similar power dependence on pump laser polarization for the off-resonance blue beam. Pump beam polarization determines the distribution of atoms

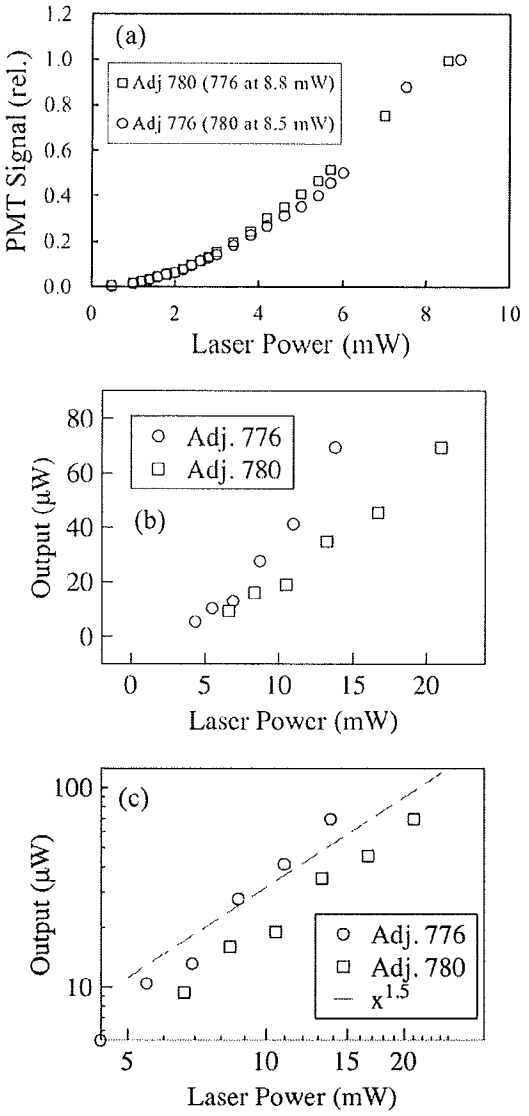

Fig. 8. Blue-beam power as a function of input power of the 780-nm and 776-nm lasers for: (a) the on-resonance beam in the Mayer laboratory, (b) the off-resonance beam in the Dawes laboratory, (c) the off-resonance beam shown on a logarithmic plot.

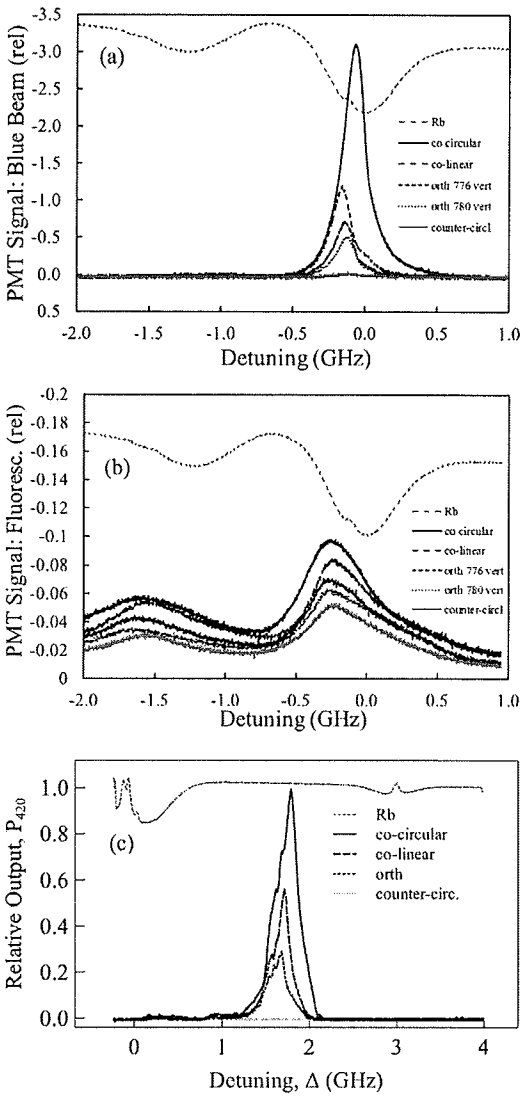

Fig. 9. (a) Blue-beam output scan for different incident laser polarizations for the on-resonance blue beam. (b) Blue fluorescence spectra for different incident laser polarizations. (c) Blue-beam output scan for different incident laser polarizations for the off-resonance beam. The rubidium absorption spectrum is included in each figure for reference.

among the hyperfine and Zeeman sub-levels of the excited 5D level. In the case of co-circular polarization, the excited atoms become concentrated in a few specific Zeeman sub-levels—those with the maximum $|m_F|$; relaxation then occurs via specific sub-levels. As an example, from the ^{85}Rb $5D_{5/2}$ ($F'=5$, $m_F=+5$) state, the relaxation process occurs via two specific states: the $6P_{3/2}$ ($F'=4$, $m_F=+4$) and the $5S_{1/2}$ ($F=3$, $m_F=+3$). These transition pathways have the highest probabilities and thus lead to the strongest output signal.[28] In contrast to the collimated blue beam, the fluorescence process is less sensitive to these particular conditions as the process is not phase-matched; the transitions involved need not satisfy the same requirements for momentum conservation.

V. SUMMARY

We have described an advanced undergraduate laboratory experiment to generate and characterize collimated blue light in rubidium vapor. Two grating-feedback diode lasers are used to drive the 5S-5P-5D ladder transition in rubidium and up to 110 μW of CBL (420 nm) is generated by frequency up-conversion. Spatial coherence of the beam is investigated via two-slit interference, and the beam power is characterized as a function of the adjustable experimental parameters. This experiment brings a contemporary field of research in nonlinear optics and quantum coherence into the undergraduate laboratory while utilizing equipment commonly available in laboratories that perform traditional optical spectroscopy experiments in rubidium vapor.

ACKNOWLEDGMENTS

The authors gratefully acknowledge the support of the M. J. Murdock Charitable Trust, The Research Corporation for Science Advancement, Pacific Research Institute for Science and Math (Pacific University), and the University of Portland.

[1]J. Mompart and R. Corbalan, "Lasing without inversion," J. Opt. B: Quantum Semiclassical Opt. **2**, R7–R24 (2000).
[2]O. Kocharovskaya, "Amplification and lasing without inversion," Phys. Rev. **219**, 175–190 (1992).
[3]K. J. Boller, A. Imamoglu, and S. E. Harris, "Observation of electromagnetically induced transparency," Phys. Rev. Lett. **66**, 2593–2596 (1991).
[4]A. S. Zibrov, M. D. Lukin, D. E. Nikonov, L. Hollberg, M. O. Scully, V. L. Velichansky, and H. G. Robinson, "Experimental demonstration of laser oscillation with population inversion via quantum interference in Rb," Phys. Rev. Lett. **75**, 1499–1502 (1995).
[5]P. S. Bhatia, G. R. Welch, and M. O. Scully, "Laser amplification without population inversion on the D_1 line of the Cs atom with semiconductor diode lasers," J. Opt. Soc. Am. B **18**, 1587–1596 (2001).
[6]H. Wu, M. Xiao, and J. Gea-Banacloche, "Evidence of lasing without inversion in a hot rubidium vapor under electromagnetically-induced-transparency conditions," Phys. Rev. A **78**, 041802-1–4 (2008).
[7]L. V. Hau, S. E. Harris, Z. Dutton, and C. H. Behroozi, "Light speed reduction to 17 meters per second in an ultracold atomic gas," Nature **397**, 594–598 (1999).
[8]S. E. Harris and Y. Yamamoto, "Photon switching by quantum interference," Phys. Rev. Lett. **81**, 3611–3614 (1998).
[9]J. Clarke, H. Chen, and W. A. van Wijngaarden, "Electromagnetically induced transparency and optical switching in a rubidium cascade system," Appl. Opt. **40**, 2047–2051 (2001).
[10]H. Schmidt and R. J. Ram, "All-optical wavelength converter and switch based on electromagnetically induced transparency," Appl. Phys. Lett. **76**, 3173–3175 (2000).
[11]A. S. Zibrov, M. D. Lukin, L. Hollberg, and M. O. Scully, "Efficient frequency up-conversion in resonant coherent media," Phys. Rev. A **65**, 051801-1–5 (2002).
[12]T. Meijer, J. D. White, B. Smeets, M. Jeppesen, and R. E. Scholten, "Blue five-level frequency-upconversion system in rubidium," Opt. Lett. **31**, 1002–1004 (2006).
[13]A. Vernier, S. Franke-Arnold, E. Riis, and A. S. Arnold "Enhanced frequency up-conversion in Rb vapor," Opt. Exp. **18**, 17020–17026 (2010).
[14]J. T. Schultz, S. Abend, D. Doring, J. E. Debs, P. A. Altin, J. D. White, N. P. Robins, and J. D. Close, "Coherent 455 nm beam production in a cesium vapor," Opt. Lett. **34**, 2321–2323 (2009).
[15]A. M. Akulshin, A. A. Orel, and R. J. McLean, "Collimated blue light enhancement in velocity-selective pumped Rb vapour," J. Phys. B **45**, 015401-1–7 (2012).
[16]K. B. MacAdam, A. Steinbach, and C. Wieman, "A narrow-band tunable diode laser system with grating feedback, and a saturated absorption spectrometer for Cs and Rb," Am. J. Phys. **60**, 1098–1110 (1992).
[17]C. Leahy, J. T. Hastings, and P. M. Wilt, "Temperature dependence of Doppler-broadening in rubidium: An undergraduate experiment," Am. J. Phys. **65**, 367–371 (1997).
[18]D. A. Van Baak, "Resonant Faraday rotation as a probe of atomic dispersion," Am. J. Phys. **64**, 724–735 (1996).
[19]K. G. Libbrecht and M. W. Libbrecht, "Interferometric measurement of the resonant absorption and refractive index in rubidium gas," Am. J. Phys. **74**, 1055–1060 (2006).
[20]A. J. Olson, E. J. Carlson, and S. K. Mayer, "Two-photon spectroscopy of rubidium using a grating-feedback diode laser," Am. J. Phys. **74**, 218–223 (2006).
[21]N. Belcher, E. E. Mikhailov, and I. Novikova, "Atomic clocks and coherent population trapping: Experiments for undergraduate laboratories," Am. J. Phys. **77**, 988–998 (2009).
[22]A. J. Olson and S. K. Mayer, "Electromagnetically induced transparency in rubidium," Am. J. Phys. **77**, 116–121 (2009).
[23]M. D. Matlin and D. J. McGee, "Photorefractive nonlinear optics in the undergraduate physics laboratory," Am. J. Phys. **65**, 622–634 (1997).
[24]K.-E. Peiponen, R. Uma Maheswari, T. Jaaskelainen, and C. Gu, "Demonstrating nonlinear optical phenomena with Chinese tea," Am. J. Phys. **61**, 937–938 (1993).
[25]D. C. Haueisen, "Description of nonlinear optics on an atomic scale," Am. J. Phys. **41**, 1251–1254 (1973).
[26]P. K. Ghosh and P. P. Banerjee, "A simplified physical picture of phase conjugation using k-space formalism and ray optics," Am. J. Phys. **61**, 237–242 (1993).
[27]The identification of commercial suppliers and part numbers is given to provide thorough details. This identification is not intended as an endorsement or recommendation of these particular suppliers; alternate suppliers might provide similar equipment that meets or exceeds the performance of the equipment listed.
[28]A. M. Akulshin, R. J. McLean, A. I. Sidorov, and P. Hannaford, "Coherent and collimated blue light generated by four-wave mixing in Rb vapour," Opt. Exp. **17**, 22861–22870 (2009).
[29]B. E. A. Saleh and M. C. Teich, *Fundamentals of Photonics* (Wiley, New York, 1991), p. 740.
[30]M. O. Scully and M. S. Zubairy, *Quantum Optics* (Cambridge, New York, 1997), p. 160.
[31]G. Morigi, S. Frnake-Arnold, and G. Oppo, "Phase-dependent interaction in a four-level atomic configuration," Phys. Rev. A **66**, 053409-1–9 (2002).
[32]J. E. Bjorkholm and P. F. Liao, "Line shape strength of two-photon absorption in an atomic vapor with a resonant or nearly resonant intermediate state," Phys. Rev. A **14**, 751–760 (1976).
[33]J. J. Maki, N. S. Campbell, C. M. Grande, R. P. Knorpp, and D. H. McIntyre, "Stabilized diode-laser system with grating feedback and frequency-offset locking," Opt. Commun. **102**, 251–256 (1993).
[34]A. S. Arnold, J. S. Wilson, and M. G. Boshier, "A simple extended-cavity diode laser," Rev. Sci. Instrum. **69**, 1236–1239 (1998).
[35]C. J. Hawthorn, K. P. Weber, and R. E. Scholten, "Littrow configuration tunable extended cavity diode laser with fixed direction output beam," Rev. Sci. Instrum. **72**, 4477–4499 (2001).
[36]A. Hemmerich, D. H. McIntyre, D. Schropp, Jr., D. Meschede, and T. W. Hänsch, "Optically stabilized narrow linewidth semiconductor laser for high resolution spectroscopy," Opt. Commun. **75**, 118–122 (1990).
[37]C. C. Bradley, J. Chen, and R. G. Hulet, "Instrumentation for stable operation of laser diodes," Rev. Sci. Instrum. **61**, 2097–2101 (1990).
[38]R. S. Conroy, A. Carleton, A. Carruthers, B. D. Sinclair, C. F. Rae, and K. Dholakia, "A visible extended cavity diode laser for the undergraduate laboratory," Am. J. Phys. **68**, 925–931 (2000).
[39]Examples include New Focus Tunable Laser TLB-6312, Thorlabs tunable laser TL780-T, Thorlabs laser diode current controller LDC201U, Thorlabs temperature controller TED200, MogLabs MOGbox, and Stanford Research Systems LDC501.